Catalysis Science & Technology

ROYAL SOCIETY OF CHEMISTRY

PAPER

View Article Online
View Journal | View Issue

Cite this: *Catal. Sci. Technol.*, 2024, **14**, 2250

High-temperature stable hydroxyls tuning the local environment of Pt single atoms for boosting formaldehyde oxidation†

Mingyi Xiao,‡[a] Lina Zhang,‡[b] Shuzhe Zheng,‡[a] Ling Fang,[a] Tulai Sun,[a] Yonghe Li,[a] Mingwu Tan,[c] Jianghao Zhang,[d] Yihan Zhu,[a] Jinshu Tian *[a] and Haifeng Xiong *[b]

Received 24th January 2024,
Accepted 9th March 2024

DOI: 10.1039/d4cy00104d

rsc.li/catalysis

The relationship between the structure and performance of metal single-atom catalysts remains elusive because it is a challenge to tailor the local environments of single atoms (SAs) while keeping the atomic dispersion. Here, two Pt/CeO_2 catalysts with different Pt coordination environments were prepared at high temperatures, *via* both atom trapping (Pt_1/CeO_2-AT) and thermal shock (Pt_1/CeO_2-TS), respectively. The Pt SAs in the Pt_1/CeO_2-TS catalyst with an unsymmetrical structure surrounded by stable surface hydroxyls exhibit excellent HCHO oxidation activity. Pt SAs are primarily found at Ce substitution sites in the Pt_1/CeO_2-TS catalyst, which has a Pt_1O_3 configuration with hydroxyls and more active surface lattice oxygen than the Pt_1/CeO_2-AT catalyst. Due to their different coordination and redox properties, Pt_1/CeO_2-TS and Pt_1/CeO_2-AT show different performances in HCHO oxidation (T_{100} of HCHO shifts from 60 to 200 °C), confirming that the catalytic performance of Pt SACs can be tailored by optimizing the local environment *via* high-temperature stable hydroxyls.

1. Introduction

Environmental catalysis has been attracting much attention because of the emission of pollutants such as aromatics and hydrocarbons. Noble metal catalysts have played a vital role in reducing these environmental pollutants, but their widespread use has been curbed due to their prohibitive cost. Given that each noble metal atom can serve as an active site in catalysis, metal single-atom catalysts (SACs) provide the opportunity for using noble metals with less capital investment. Recently, some metal SACs have been reported to exhibit high reactivity in pollutant mitigation such as the oxidation of volatile organic compounds.[1–3]

Much progress has been made in the preparation of metal SACs, such as the approaches of coprecipitation, atomic layer deposition (ALD),[4] atom trapping[5] and vapor-phase self-assembly.[6] However, when compared to nano-cluster/particle catalysts, SACs are not always active in catalytic reactions because of the unfavorable coordination structure of metal single atoms. Fine-tuning the oxidation states or local environments of SACs has the potential to significantly improve their performance in catalysis.[7–12] In CO oxidation, several strategies have been employed to generate metal single atoms with improved catalytic performance. For example, steam-treatment of a Pt_1/CeO_2 catalyst enabled the generation of hydroxyl groups adjacent to Pt single atoms, leading to a dramatic activity increase in CO oxidation due to the generation of surface active lattice oxygen.[13] The use of a highly defective CeO_2–Al_2O_3 support can tune the oxidation state of Pt_1 and enhance catalytic activity in CO, CH_4, and NO oxidation.[12] Recently, Li *et al.* grafted isolated and defective CeO_x nanoglue islands onto SiO_2, hosting one Pt atom on average. This catalyst exhibits significantly increased activity for CO oxidation.[14] Furthermore, using a simple calcination temperature-control strategy, Tan *et al.* fabricated CeO_2 supported Pt_1 with precisely controlled coordination environments, and its activity trend in CO oxidation and NH_3 oxidation is reversed due to the different property in reactant activation and H_2O desorption.[8] In addition, O_2 plasma leads to the formation of surface peroxo

[a] *College of Chemical Engineering, Zhejiang University of Technology, Hangzhou, 310014, China. E-mail: tianjs@zjut.edu.cn*
[b] *College of Chemistry and Chemical Engineering, State Key Laboratory for Physical Chemistry of Solid Surfaces, Xiamen University, Xiamen, 361005, China. E-mail: haifengxiong@xmu.edu.cn*
[c] *Institute of Sustainability for chemicals, Energy and Environment, Agency for Science, Technology and Research (A*STAR), 1 Pesek Road, Jurong Island, 627833, Singapore*
[d] *State Key Joint Laboratory of Environment Simulation and Pollution Control, Research Center for Eco-environmental Sciences, Chinese Academy of Sciences, Beijing, 100085, China*

† Electronic supplementary information (ESI) available. See DOI: https://doi.org/10.1039/d4cy00104d

‡ These authors contributed equally to this work.

(O_2^{2-}) structures that facilitate the formation of strongly bonded Pt^{2+} atoms, rendering them active and resistant to sintering in the CO oxidation reaction.[15] These Pt_1/CeO_2 catalysts were prepared at low temperatures, involving the effect of various kinds of surface functionals such as hydroxyls.[16] The presence of various hydroxyls therefore masked the identification of the structure–performance relationship when investigating the effect of local coordination environments of metal single atoms in catalysis. In addition, the distance between a single metal atom and a hydroxyl group is crucial in determining the formation of active intermediates, which in turn impacts the catalytic performance in catalysis. For example, Wu *et al.* recently discovered that the closeness between the OH group and a single Rh atom on a plane surface significantly influences the catalytic activity of the Rh_1/CeO_2 single-atom catalyst system in CO oxidation.[17]

In this work, we focus on the high-temperature preparation of Pt_1/CeO_2 single-atom catalysts to avoid the effect of different kinds of hydroxyl groups because high temperature treatment can remove the weakly adsorbed hydroxyls, only leaving the strongly bonded hydroxyls behind. We employed two high-temperature approaches, *i.e.*, atom trapping (AT) and thermal shock (TS), to prepare Pt_1/CeO_2 catalysts. The Pt/CeO_2 SAC prepared by atom trapping (Pt_1/CeO_2-AT) is achieved by ramping the temperature to 800 °C in air and keeping at that temperature for 10 h, and the Pt/CeO_2 SAC prepared by thermal shock (Pt_1/CeO_2-TS) is achieved by thermally shocking the sample to ~1000 °C for ~0.5 s and repeating the process multiple times. The catalytic performances of the Pt_1/CeO_2 catalysts were then investigated in formaldehyde oxidation and the function of the local environment of the Pt single atoms was studied.

2. Experimental section

2.1 Material preparation

Cerium(III) nitrate hexahydrate ($Ce(NO_3)_3{\cdot}6H_2O$, ≥99.99%) was purchased from Alfa Aesar. Chloroplatinic acid hexahydrate ($H_2PtCl_6{\cdot}6H_2O$, Pt ≥ 37.5%) was purchased from Sinopharm Chemical Reagent Limited Corporation. Briefly, 1 g of chloroplatinic acid hexahydrate powder was dissolved in 10 mL of deionized water to prepare a chloroplatinic acid solution. $Ce(NO_3)_3{\cdot}6H_2O$ was calcined in air at 350 °C for 2 h to obtain CeO_2, which was used as the support to prepare Pt_1/CeO_2 catalysts. All the reagents were used as received.

The Pt_1/CeO_2-AT single-atom catalyst was prepared *via* atom trapping (AT).[13] A 1.0 wt% Pt/CeO_2 catalyst was synthesized by the incipient wetness impregnation method. An appropriate amount of chloroplatinic acid solution was added dropwise to CeO_2 while being kept grinding in a mortar and pestle. Then, the obtained mixture was dried at 80 °C for 12 h in static air and calcined in a muffle furnace at 800 °C for 6 h at a temperature increase rate of 10 °C min^{-1}. The resulting catalyst powder was denoted as Pt_1/CeO_2-AT.

The Pt_1/CeO_2-TS single-atom catalyst was prepared *via* thermal-shock (TS).[11] The TS synthesis features a high temperature, but very short heating duration operated in an inert atmosphere. Specifically, a thin layer of the dried Pt/CeO_2 precursor powder was uniformly spread out into a graphite plate and rapidly heated to a high temperature and then quenched through a carbon heater using Joule heating equipment (Hefei *in situ* Technology Co., Ltd. China). The temperature was monitored to be around 1000 °C for ~0.5 s. The pulse power was about 300 Å × 40 V. This thermal shock process was repeated 6 times, and before each heating, the Pt/CeO_2 precursor powder was mixed to ensure uniform heating and single atom formation. The resulting catalyst was denoted as Pt_1/CeO_2-TS.

2.2 Catalytic activity measurements

The HCHO oxidation reaction was carried out in a fixed-bed quartz flow reactor (i.d. = 7.0 mm) under atmospheric pressure. Briefly, 80 mg catalyst (40–60 mesh) was mixed with 120 mg quartz sand. After placing in the quartz tube reactor, the feed gas composition of 400 ppm HCHO/20% O_2/N_2 was introduced and the total flow rate was kept at 50 mL min^{-1}. Water vapor was generated by introducing liquid water into a vaporizer using a Cole Parmer 74900 syringe pump and carried into the reactor by N_2. To investigate the moisture effect, relative humidity (20%) was achieved by adjusting the injection speed of the pump. The products in the effluent gas were analyzed using an online gas chromatograph (GC2060, Shanghai Ruimin GC Instruments Inc.), which was described in previous work.[18]

2.3 Characterization

Details of the characterization of the catalysts are described in the ESI.†

3. Results and discussion

3.1 Microstructure characterization of materials

Atom trapping (AT) and thermal shock (TS) methods were used to prepare Pt_1/CeO_2-AT and Pt_1/CeO_2-TS catalysts with a Pt loading of 1.0 wt%. The powder X-ray diffraction (XRD) patterns of the two catalysts (Fig. S1†) only show the diffraction peaks of ceria (JCPDS No.34-0394), without the diffraction peaks of metallic Pt or PtO_2. X-ray photoelectron spectroscopy (XPS) in the Pt 4f region revealed that Pt remained as the ionic form of Pt^{2+} (72.4 eV and 75.8 eV) over both catalysts (Fig. S2†) without the existence of Pt^0 and Pt^{4+} species.[19,20] High-angle annular dark-field scanning transmission electron microscopy (HAADF-STEM) images revealed the presence of Pt single atoms dispersed on the CeO_2 support in the Pt_1/CeO_2-AT and Pt_1/CeO_2-TS (Fig. 1A and B and Fig. S3†) catalysts, without the presence of Pt clusters or nanoparticles, confirming the high dispersion of Pt single atoms (SAs). This suggests that the atomic

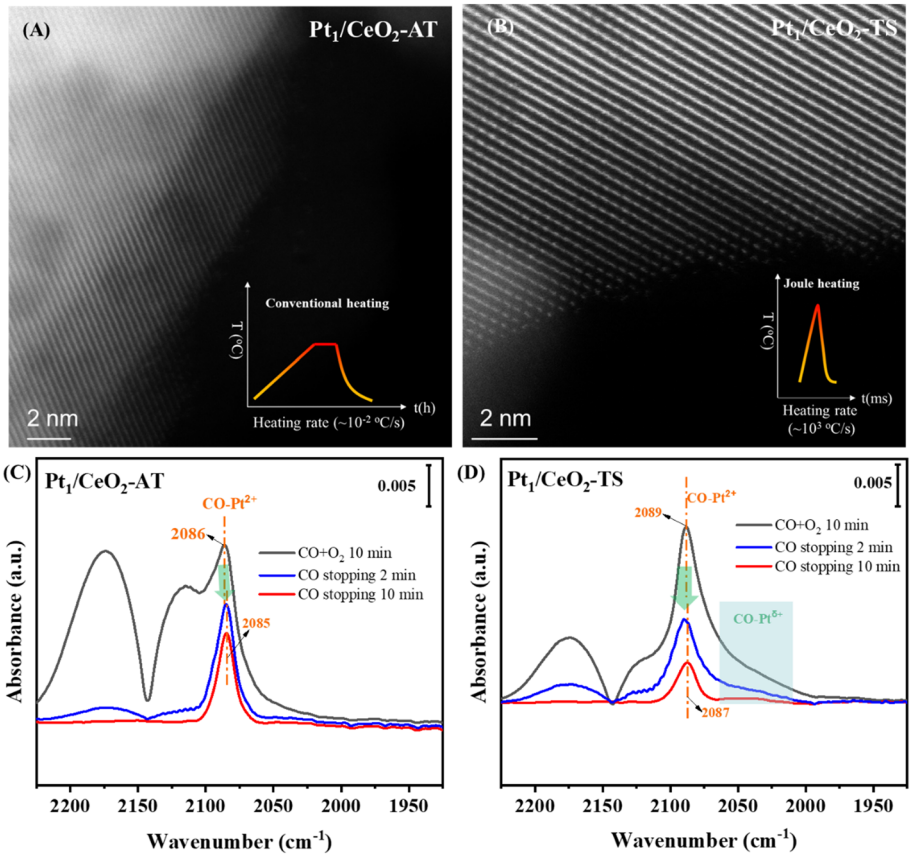

Fig. 1 Representative AC-STEM images of the obtained Pt_1/CeO_2-AT (A) and Pt_1/CeO_2-TS (B) catalysts, and the CO-DRIFT spectra of the Pt_1/CeO_2-AT (C) and Pt_1/CeO_2-TS (D) catalysts at 120 °C (CO-DRIFT experiments were performed by the following steps. Step 1: $CO/O_2/He$ was first introduced into the cell for 10 min; step 2: the CO flow was stopped while O_2/He was kept flowing for 10 min).

dispersion of Pt^{2+} was present on both Pt_1/CeO_2-AT and Pt_1/CeO_2-TS catalysts.

Diffuse reflectance infrared Fourier transform spectroscopy (DRIFTS) using CO as a probe molecule (CO-DRIFTS) was used to figure out the local environment of the two Pt_1/CeO_2 SACs. Fig. 1C and D reveal that the two catalysts present isolated Pt species, as confirmed by the CO bands at 2086 and 2089 cm^{-1}, which is consistent with the XPS and HAADF-STEM results. The spectra do not show the lower-wavenumber features (<2000 cm^{-1}) assigned to the bridge or three-fold adsorbed CO on Pt clusters or nanoparticles,[21,22] further indicating the atomic dispersion of the Pt species on the two Pt_1/CeO_2 catalysts. The different peaks between 2000 and 2090 cm^{-1} of the two catalysts indicate the different local environments (*e.g.*, location or coordination structure) of Pt single atoms. Pt_1/CeO_2-TS shows a more intense CO–Pt^{2+} (~2089 cm^{-1}) peak and a broader CO–$Pt^{\delta+}$ (~2052 cm^{-1}) peak, suggesting the wide distribution of local environments of Pt^{2+} with an unsaturated coordination configuration,[8,22] which is also evidenced by density functional theory (DFT) simulation below. The simulations in Fig. S4† showed that as the Pt–O coordination number decreased on the Pt_1/CeO_2 (111) model, the vibrational frequency decreased from 2123.7 to 2028.2 cm^{-1}. This corroborates that the Pt atoms on Pt_1/CeO_2-TS are likely coordinated with less adjacent heteroatoms. Along with the peak at ~2086 cm^{-1} assigned to CO on Pt^{2+} species with a square-planar Pt_1O_4 configuration, there is no obvious peak at 2052 cm^{-1} for Pt_1/CeO_2-AT, implying that Pt_1/CeO_2-AT contains very few less-coordinated Pt single atoms, which agrees well with the previous result.[11,22]

The local coordination environment and the oxidation state of Pt single atoms were further investigated by X-ray absorption spectroscopy (XAS) at the Pt L_3-edge.[23,24] Fig. 2A shows the XANES spectra of the reference Pt foil and Pt_1/CeO_2 catalysts. The spectral analysis of Pt_1/CeO_2-TS closely resembles that of Pt_1/CeO_2-AT, which has been previously confirmed to consist of isolated platinum species carrying a +2 state.[11,15,22] Because of the absence of Pt–Pt scattering in the EXAFS spectrum (Fig. 2C), the Pt species on Pt_1/CeO_2-TS is therefore the isolated Pt^{2+} cation, which is also confirmed by XPS (Fig. S2†). It is noted that Pt_1/CeO_2-TS shows a slightly lower white line intensity as compared to Pt_1/CeO_2-AT (Fig. 2B), indicating that the ionic Pt^{2+} on the former is a less saturated coordination.[13] Furthermore, in the XANES absorption edge of Pt_1/CeO_2-TS, a rising-edge feature was observed, demonstrated by a bump in the first-order derivative curve (Fig. 2B). Such a rising edge is due to the

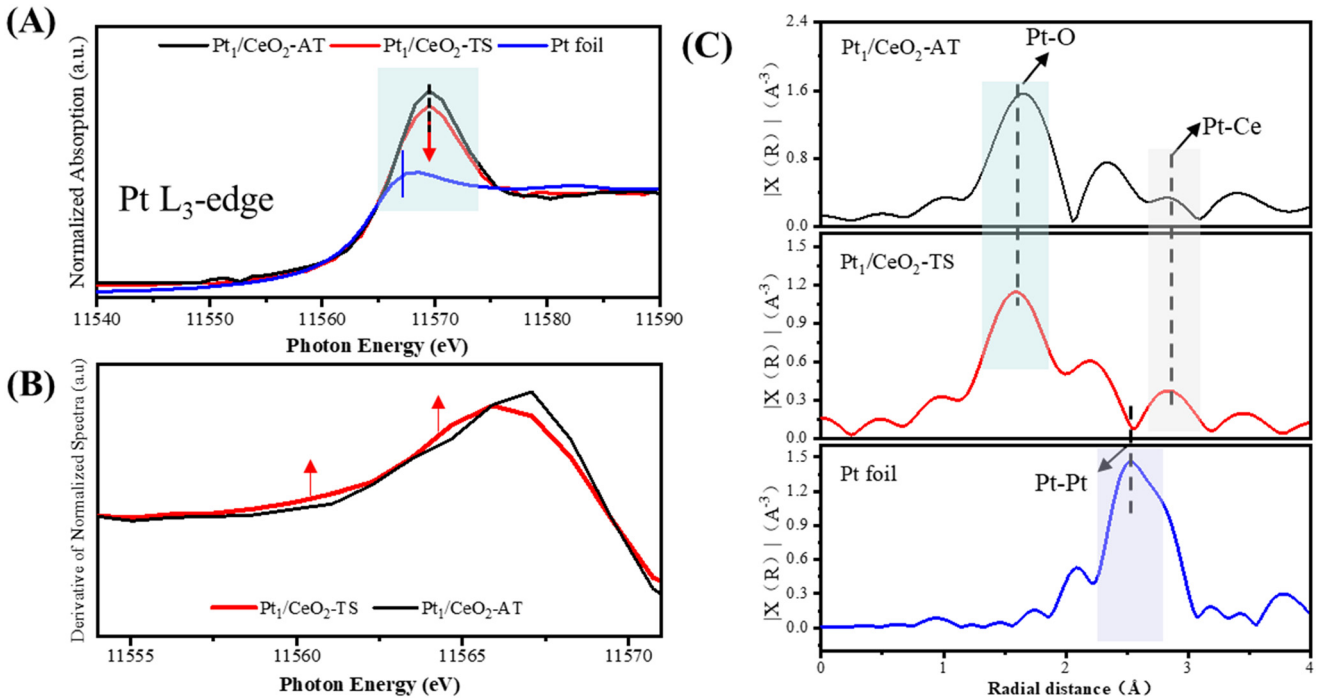

Fig. 2 The XAS analysis of the Pt samples demonstrating the different coordination environments of Pt single atoms over the Pt_1/CeO_2 SACs. (A) Normalized XANES spectra, (B) the first derivative of the normalized XANES spectra in (A) and (C) EXAFS magnitude of the Fourier transformed k^2-weighted $\chi(k)$ data for Pt_1/CeO_2-AT (black) and Pt_1/CeO_2-TS (red) at the Pt-L_3 edge. The reference Pt foil (blue) was used for XANES analysis.

decreased local coordination symmetry of the Pt.[25] This confirms that the TS technique produces the Pt_1/CeO_2-TS catalyst having isolated Pt^{2+} species with an unsaturated coordination configuration, which were analyzed by fitting the EXAFS spectra (Fig. S5 and Table S2†). The Pt_1/CeO_2-AT catalyst presents a square-planar Pt_1O_4 configuration with four equivalent Pt–O bonds, as revealed in previous work.[26,27] However, Pt_1/CeO_2-TS has a relatively low Pt–O coordination number (CN) of approximately 3.6 (Table S2†), indicating a defective Pt_1O_x ($x < 4$) configuration. It is known that the square-planar PtO_4 has high thermal stability, whereas the low-coordinated Pt_1O_x in the air-exposed state is less stable. The improved stability of Pt_1O_x is therefore proposed to be related to the hydroxyl existing on the surface at high temperature.[13,16] To verify the existence of the high-temperature stable hydroxyl, we performed the deconvolution of the O 1s XPS spectra for both samples, which included three peaks (Fig. S6†). The peaks at ~528.9, 530.8 and 531.6 eV are assigned to the lattice oxygen (O_L), defect-related oxygen (O_D) and surface hydroxyl oxygen (O_{OH}), respectively.

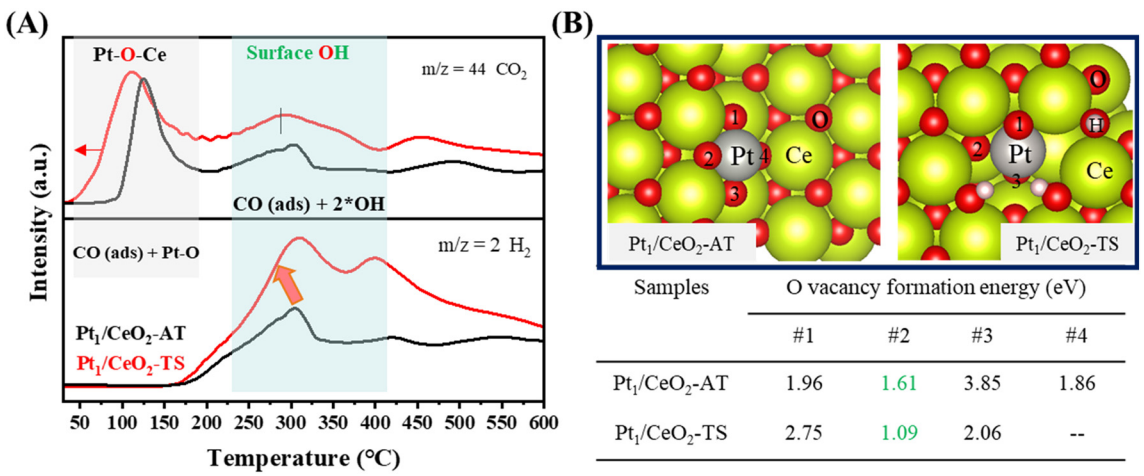

Samples	O vacancy formation energy (eV)			
	#1	#2	#3	#4
Pt_1/CeO_2-AT	1.96	1.61	3.85	1.86
Pt_1/CeO_2-TS	2.75	1.09	2.06	--

Fig. 3 (A) CO-TPR profiles of the Pt_1/CeO_2-AT and Pt_1/CeO_2-TS catalysts, CO_2 (m/z = 44) and H_2 (m/z = 2) signals. (B) A top-down view of the PtO_x active site on the surface of CeO_2 (111), with atoms close to the Pt atom and the corresponding formation energy of the O-vacancy.

Therefore, we deduced that compared to the Pt_1/CeO_2-AT sample with a square-planar Pt_1O_4 coordination, a non-equilibrium Pt_1O_x configuration stabilized by the surface hydroxyl on the CeO_2 (111) facet was formed on the Pt_1/CeO_2-TS catalyst during the TS treatment, which is confirmed by the FTIR result (Fig. S7†). The data shown in Fig. S7† clearly indicate that the Pt_1/CeO_2-TS catalyst exhibits unique vibrational peaks around 3500 cm^{-1}, which we can associate with surface hydroxyl groups. This finding further supports and confirms our initial theory.

The oxygen-containing surface species on the catalysts were further characterized by CO temperature-programmed reduction (CO-TPR) (Fig. 3A). As for Pt_1/CeO_2-AT, the surface lattice oxygen in the vicinity of Pt (Pt–O–Ce bond) can react with CO at ~90 °C, while on the Pt_1/CeO_2-TS catalyst, it can not only react with CO at a lower temperature (~50 °C) but also produce more CO_2, suggesting that surface oxygen species are more active and abundant on the latter. Meanwhile, more surface hydroxyl groups were generated on the Pt_1/CeO_2-TS catalyst, which can react with CO at ~175 °C. The effect of surface hydroxyls was rarely considered in previous studies on Pt_1/CeO_2-AT,[23,28,29] primarily because those formed by AT are far away from the active sites and have little influence on the local environment of the active single atoms.[13,16] Surface hydroxyls were found to be more abundant in Pt_1/CeO_2-TS, correlating with the XPS results. Simultaneously, these surface hydroxyls had a lower reaction temperature than those formed from AT and a similar reaction temperature to hydroxyls formed by high-temperature steam treatment,[13,16,30] implying that the hydroxyl groups on Pt_1/CeO_2-TS could affect the local environment of Pt single atoms. This lends credence to the hypothesis that surface hydroxyls produced from TS can stabilize single atoms. We also found the presence of more oxygen defects at Pt_1/CeO_2-TS (Fig. S8†), which agrees well with the results of EXAFS and CO-DRIFTS. Raman spectroscopy (Fig. S9†) revealed the formation of the Pt–O–Ce bond, as evidenced by the feature of the peak at 550 cm^{-1} (the one at 657 cm^{-1} corresponding to Pt–O). The significant decrease in the peak strength of the Pt_1/CeO_2-TS catalyst is due to the looser bonds of Ce–O–Ce and Pt–O–Ce as compared to the Pt_1/CeO_2-AT sample, which also confirms that the surface oxygen is more active *via* TS treatment.[31,32] Models of Pt_1/CeO_2-TS and Pt_1/CeO_2-AT were built based on the characterization results and are shown in Fig. 3B. The model for the Pt_1/CeO_2-AT catalyst is a symmetric square-planar Pt_1O_4 coordination, whereas the structure model of Pt_1O_3 on CeO_2 (111) stabilized with surface hydroxyls is built for the Pt_1/CeO_2-TS catalyst.[11] For the PtO_3 model, the formation energy of the oxygen vacancy is lower than that of the square-planar Pt_1O_4 ensemble (1.09 *vs.* 1.61 eV). Since the formation energy of the O-vacancy of the low-coordination PtO_2 is greater than that of the square-planar Pt_1O_4 coordination (2.21 *vs.* 1.61 eV), which contradicts the CO-TPR and EXAFS results, the local environment of the Pt single atoms in the Pt_1/CeO_2-TS catalyst is therefore determined as the non-equilibrium PtO_3 configuration surrounded with the surface hydroxyls existing at high temperature.

3.2 Evaluation performance of HCHO oxidation

We tested the two Pt_1/CeO_2 catalysts prepared at high temperatures in HCHO oxidation to evaluate their distinct catalytic performance in environmental catalysis. The Pt_1/CeO_2-AT catalyst has a high onset temperature of ~120 °C and achieves only 50% HCHO conversion at 170 °C (Fig. 4A). However, the Pt_1/CeO_2-TS catalyst exhibits low-temperature activity, achieving 100% HCHO conversion at 60 °C. The turnover frequencies (TOFs) of the Pt_1/CeO_2-TS catalyst in formaldehyde catalytic oxidation can reach up to approximately 8.5 per hour at room temperature. This level of activity is relatively impressive compared to other catalytic systems based on Pt for similar reaction conditions, as indicated in Table S3.† Moreover, the Pt_1/CeO_2-TS catalyst demonstrated excellent stability in a time-on-stream run of 50 h in the presence of 400 ppm HCHO at 30 °C (Fig. S10†). The spent Pt_1/CeO_2-TS catalyst after 50 h of HCHO oxidation (Pt_1/CeO_2-TS-spent) was characterized, and the HAADF-STEM (Fig. S11A, B and S13†), XRD (Fig. S11C†), Raman (Fig. S11D†) and XPS results (Fig. S11E and F†) confirmed that there are no significant changes in the CeO_2 morphology and Pt local environments. Furthermore, the surface Ce species (Fig. S11E†), oxygen defects and hydroxyl groups (Fig. S12†) have no obvious changes after the reaction, which is consistent with the *in situ* HCHO-DRIFTS results below (Fig. 5), demonstrating that the surface hydroxyls were maintained.

In addition, the effect of relative humidity (RH) on HCHO catalytic oxidation was investigated. As seen in Fig. 4B, under 20% relative humidity, the reactivity of Pt_1/CeO_2-TS is higher than that under dry conditions (~80% *vs.* ~65%). The previous studies have reported that the presence of H_2O significantly improves the transformation of dioxymethylene (DOM, H_2COO) into formate species (HCOO) or promotes the adsorption of formaldehyde and the formation of HCOO species. Therefore, the presence of an appropriate amount of water vapor can enhance the oxidation of HCHO, indicating the good tolerance of the Pt_1/CeO_2-TS catalyst against moisture. Therefore, the Pt_1/CeO_2-TS catalyst exhibits superior activity and excellent durability in the mitigation of HCHO.

3.3 Reaction mechanism and theoretical calculation

To investigate the reaction mechanism and the efficient activation of HCHO and O_2 molecules over the Pt_1/CeO_2-TS catalyst, we performed *in situ* HCHO-DRIFTS experiments and DFT calculations. The *in situ* HCHO-DRIFTS experiments were carried out on the Pt_1/CeO_2-TS catalyst in a flow of HCHO/N_2 or HCHO/O_2/N_2 (Fig. 5) at room temperature to gain insight into the formation of intermediates during the reaction. As shown in Fig. 5, with the introduction of HCHO/N_2 or HCHO/O_2/N_2, there was no peak associated with the

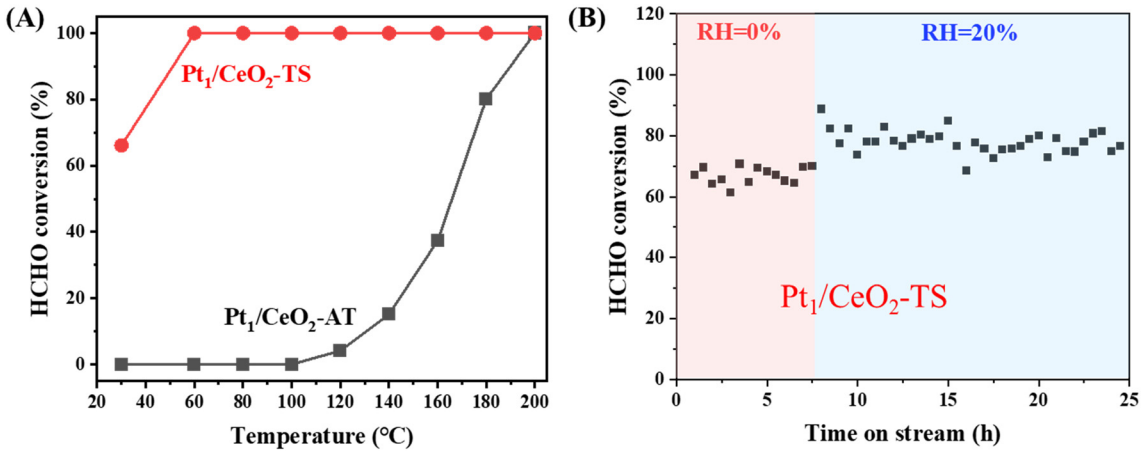

Fig. 4 (A) HCHO conversion as a function of temperature over the Pt_1/CeO_2-AT and Pt_1/CeO_2-TS single-atom catalysts. (B) Relative humidity effect (20%) on the activity of the Pt/CeO_2-TS catalyst at 30 °C. The reaction conditions were described in the Experimental section.

adsorbed HCHO (1722 cm^{-1}) on the Pt_1/CeO_2-TS catalyst.[33] The assignments of other peaks appeared are listed in Table S4.† It should be noted that with the introduction of HCHO/N_2 from 20 to 40 min (Fig. 5), the contents of HCOO and DOM species gradually increase, while the adsorption peak at 3695 cm^{-1} becomes more negative (Fig. 5), which is assigned to the consumption of the hydroxyl species residing on the catalyst at high temperature.[34,35] This indicates that the formation of surface DOM and HCOO consumes the surface hydroxyls. At the same time, we found that the intensity of the DOM peak formed during the entire HCHO/N_2 process was significantly higher compared to that of the HCOO species. This result contradicts the previous findings on a steam-treated Pt_1/CeO_2 catalyst having surface hydroxyls,[16] indicating a different reaction mechanism. When the reactant gas was switched to HCHO/O_2/N_2, the DOM and HCOO species were still present, whereas their intensity was much lower than that in HCHO/N_2. The decrease of DOM and HCOO peaks indicates that oxygen is needed for further dehydrogenation. The peak position and intensity of the surface hydroxyl group did not change significantly throughout the catalytic cycle, which suggests that the consumption of the surface hydroxyl group was a reversible process that primarily facilitated the adsorption of intermediate species rather than breaking the C–H bond. We propose that the main reaction path in the Pt_1/CeO_2-TS catalyst is HCHO* → DOM* → HCOO* → COO*. Previous studies have already proposed that the reaction mechanism involves the decomposition of HCOO* into *CO, followed by its subsequent oxidation into *CO_2. To reinforce the credibility and validity of our proposed mechanism, we have obtained additional supporting evidence from our *in situ* infrared analysis, specifically the absence of CO peaks. The activation of the HCHO* molecule is a two-step process, with the first step being the breaking of the C–H bond in DMO to form HCOO, mainly by surface active oxygen species, and the second step being the further breaking of the C–H bond to form COO* with the assistance of O_2 molecules. Based on the *in situ* experiments, we propose that the high-temperature stable hydroxyl on the Pt_1/CeO_2-TS catalyst promotes the adsorption activation of DMO and HCOO, and the subsequent dehydrogenation of DOM to HCOO is the rate-limiting step of the whole reaction. Furthermore, the O_2 molecule is easily activated by the Pt_1/CeO_2-TS catalyst to rapidly break C–H bonds.

DFT simulation is used to further validate the reaction mechanism and the activation of reactants over the Pt_1/CeO_2-TS catalyst in HCHO oxidation. Based on the characterization, the Pt_1/CeO_2-TS model has a Pt single atom bonding with three oxygen atoms on CeO_2 (111), as well as two neighboring active hydroxyls located adjacently to the Pt atom (PtO_3–$Ce(OH)_2$), as shown in Fig. S14.† The energy barrier of each step on the optimized Pt_1/CeO_2-TS model in the reaction was calculated and is shown in Fig. 6. HCHO oxidation starts with the adsorption of HCHO at the Pt_1 site over the PtO_3–$Ce(OH)_2$ ensemble. The adsorbed HCHO reacts with the adjacent active oxygen species from the Pt–O bond to form $H_2COO^*_{lat}$ (DMO*), and meanwhile the bridging OH group interacts with O from HCHO, which stabilizes the

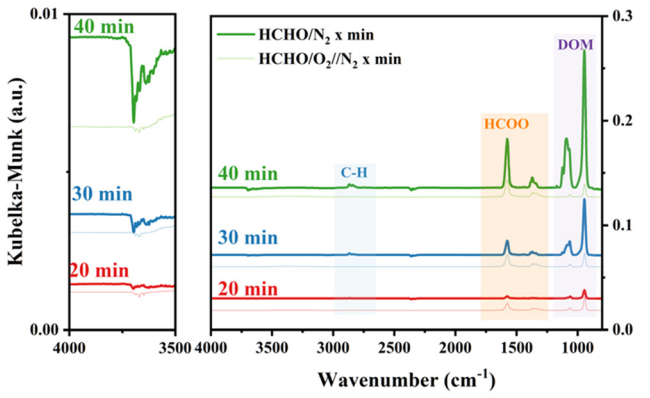

Fig. 5 *In situ* HCHO-DRIFTS of the Pt_1/CeO_2-TS catalyst carried out in a flow of HCHO/N_2 (solid line) or HCHO/O_2/N_2 (dotted line) at 30 °C.

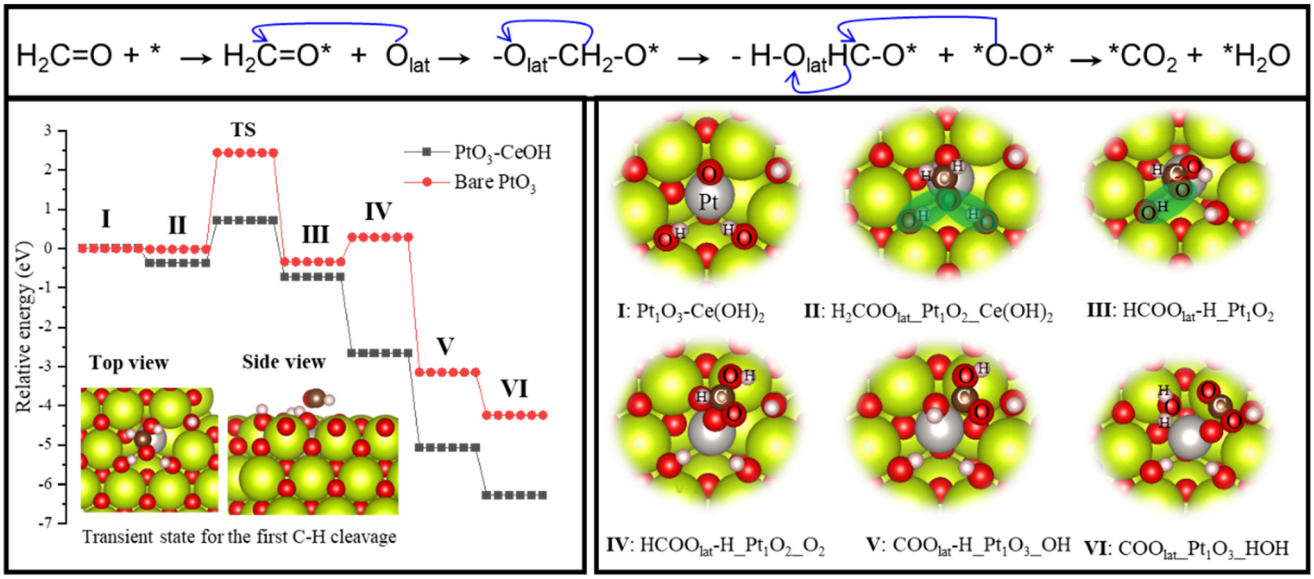

Fig. 6 The calculated energy profile and the corresponding structures of the intermediates and transition states of the key elemental steps on Pt_1O_3–$Ce(OH)_2$ on the CeO_2 (111) surface in HCHO oxidation.

$H_2COO^*_{lat}$ species. This is consistent with the results on the formation of DMO and the consumption of hydroxyls in the *in situ* DRIFTS experiment. The DFT calculation shows that this step is exothermic (−0.38 eV) with no activation barrier. Then, the formed $H_2COO^*_{lat}$ starts the first C–H bond breaking reaction, which involves the interaction of C–H with the activated Pt–O_{lat} bond to form $HCOO^*_{lat}$ and OH species. Despite being exothermic (−0.36 eV), this step has a high energy barrier of 0.88 eV. This suggests that $HCOO^*_{lat}$ species are more difficult to form as compared to $H_2COO^*_{lat}$ species, which explains the reason that the peak intensity of DMO is significantly higher than that of HCOO in the *in situ* DRIFTS experiment (Fig. 5). The activation of an oxygen molecule (O_2^*) at the surface vacancy is highly exothermic (−1.93 eV), and the O_2^* species reacts with $HCOO^*_{lat}$ to break the second C–H bond. This is a highly exothermic step (−2.41 eV) with a low energy barrier, indicating that oxygen activation is not the rate-limiting step in the reaction. This finding is consistent with the results of the *in situ* DRIFTS experiment. Finally, the interaction of COO*–H and hydroxyl species results in the formation of COO*, H_2O*, and Pt–O bonds on the CeO_2 surface, completing the reaction cycle. As a comparison, we also examined the PtO_3 structure with no hydroxyls (Fig. 6, red line and S15†). The study discovered that the first step of the C–H bond activity requires a very high activation energy (~2.5 eV), which is similar to the catalyst obtained through the AT method.[16] As confirmed by the *in situ* experiment and DFT calculation, the high-temperature stable surface hydroxyl existing from the TS synthesis primarily facilitated the adsorption activation of DMO and HCOO* and did not participate in the C–H bond breaking. The activation of C–H bonds during the HCHO oxidation reaction is influenced by the activity of surface oxygen species. The initial C–H bond activation is facilitated by the surface lattice oxygen present in the Pt–O–Ce bond, whereas the subsequent C–H bond activation is facilitated by the adsorbed oxygen species produced by molecular oxygen dissociation.

4. Conclusions

In this work, we tune the local environment of the Pt single atoms on two Pt_1/CeO_2 single-atom catalysts (SACs) prepared at elevated temperatures (>800 °C), *i.e.*, *via* atom trapping (Pt_1/CeO_2-AT) and thermal shock (Pt_1/CeO_2-TS). The use of the high-temperature preparation avoids the effect of various surface hydroxyls existing at low temperatures, exclusively maintaining the high-temperature stable hydroxyls. The Pt single atoms in the Pt_1/CeO_2-TS catalyst present the non-equilibrium local environments surrounded by high-temperature stable hydroxyls, exhibiting excellent activity in HCHO oxidation and lowering the T_{100} to 60 °C, as compared to the T_{100} of 200 °C for the Pt_1/CeO_2-AT catalyst.

For the Pt_1/CeO_2-TS catalyst, Pt single atoms substituting the Ce site of CeO_2 (111) have a Pt_1O_3 configuration coordinated with hydroxyls (Pt–O CN of 3.6), showing more active surface lattice oxygen than the Pt_1/CeO_2-AT catalyst (symmetric square-planar Pt_1O_4 coordination). The high-temperature stable hydroxyl existing on Pt_1/CeO_2-TS promotes the adsorption of formaldehyde, DMO and HCOO, but does not participate in the C–H bond activation. This confirms that the catalytic performance of Pt SACs can be tailored by tuning the local environment of Pt single atoms with the help of high-temperature stable hydroxyls. This work provides insight into preparing efficient single-atom catalysts for environmental catalysis.

Data availability statement

The data that support this study are available from the corresponding author upon reasonable request.

Author contributions

Jinshu Tian: conceptualization, investigation, methodology, writing – original draft. Mingyi Xiao and Lina Zhang: investigation, formal analysis, methodology, writing – review & editing. Shuzhe Zheng and Ling Fang: investigation, methodology, validation, visualization. Tulai Sun: visualization, investigation, writing – review & editing. Yonghe Li: writing – review & editing. Yihan Zhu: writing – review & editing. Jianghao Zhang: writing – review & editing. Haifeng Xiong: conceptualization, investigation, methodology, writing – review and editing, supervision.

Conflicts of interest

All the authors declare no conflicts of interest.

Acknowledgements

The authors thank the Shanghai Synchrotron Radiation Facility (SSRF) for providing the beamtime at the BL11B beamline. This work was financially supported by the National Natural Science Foundation of China (Grant No. 22279115), the National High-Level Talent Fund (22072118) and the Fundamental Research Funds for the Provincial Universities of Zhejiang (RF-A2023005).

References

1 S. Zhao, Y. Wen, X. Liu, X. Pen, F. Lü, F. Gao and X. Tang, Formation of active oxygen species on single-atom Pt catalyst and promoted catalytic oxidation of toluene, *Nano Res.*, 2020, **13**, 1544–1551.

2 K. Yang, Y. Liu, J. Deng, X. Zhao, J. Yang, Z. Han, Z. Hou and H. Dai, Three-dimensionally ordered mesoporous iron oxide-supported single-atom platinum: Highly active catalysts for benzene combustion, *Appl. Catal., B*, 2019, **244**, 650–659.

3 M. Jiang, D. Yan, X. Lv, Y. Gao and H. Jia, Recognition of water-dissociation effect toward lattice oxygen activation on single-atom Co catalyst in toluene oxidation, *Appl. Catal., B*, 2022, **319**, 121962.

4 Q. Q. Guan, C. W. Zhu, Y. Lin, E. I. Vovk, X. H. Zhou, Y. Yang, H. C. Yu, L. N. Cao, H. W. Wang, X. H. Zhang, X. Y. Liu, M. K. Zhang, S. Q. Wei, W. X. Li and J. L. Lu, Bimetallic monolayer catalyst breaks the activity-selectivity trade-off on metal particle size for efficient chemoselective hydrogenations, *Nat. Catal.*, 2021, **4**, 840–849.

5 R. Alcala, A. Delariva, E. J. Peterson, A. Benavidez, C. E. Garcia-Vargas, D. Jiang, X. I. Pereira-Hernandez, H. H. Brongersma, R. Ter Veen and J. Stanek, Atomically Dispersed Dopants for Stabilizing Ceria Surface Area, *Appl. Catal., B*, 2021, **284**, 119722.

6 H. C. Li, Q. Wan, C. Du, J. Zhao, F. Li, Y. Zhang, Y. Zheng, M. Chen, K. H. L. Zhang, J. Huang, G. Fu, S. Lin, X. Huang and H. Xiong, Layered Pd oxide on PdSn nanowires for boosting direct H(2)O(2) synthesis, *Nat. Commun.*, 2022, **13**, 6072.

7 J. Yang, Y. Huang, H. Qi, C. Zeng, Q. Jiang, Y. Cui, Y. Su, X. Du, X. Pan, X. Liu, W. Li, B. Qiao, A. Wang and T. Zhang, Modulating the strong metal-support interaction of single-atom catalysts *via* vicinal structure decoration, *Nat. Commun.*, 2022, **13**, 4244.

8 W. Tan, S. Xie, D. Le, W. Diao, M. Wang, K. B. Low, D. Austin, S. Hong, F. Gao, L. Dong, L. Ma, S. N. Ehrlich, T. S. Rahman and F. Liu, Fine-tuned local coordination environment of Pt single atoms on ceria controls catalytic reactivity, *Nat. Commun.*, 2022, **13**, 7070.

9 F. Dvorak, M. Farnesi Camellone, A. Tovt, N. D. Tran, F. R. Negreiros, M. Vorokhta, T. Skala, I. Matolinova, J. Myslivecek, V. Matolin and S. Fabris, Creating single-atom Pt-ceria catalysts by surface step decoration, *Nat. Commun.*, 2016, **7**, 10801.

10 J. Zhang, X. Qin, X. Chu, M. Chen, X. Chen, J. Chen, H. He and C. Zhang, Tuning Metal-Support Interaction of Pt-CeO_2 Catalysts for Enhanced Oxidation Reactivity, *Environ. Sci. Technol.*, 2021, **55**, 16687–16698.

11 D. Jiang, Y. Yao, T. Li, G. Wan, X. I. Pereira-Hernandez, Y. Lu, J. Tian, K. Khivantsev, M. H. Engelhard, C. Sun, C. E. Garcia-Vargas, A. S. Hoffman, S. R. Bare, A. K. Datye, L. Hu and Y. Wang, Tailoring the Local Environment of Platinum in Single-Atom Pt_1/CeO_2 Catalysts for Robust Low-Temperature CO Oxidation, *Angew. Chem., Int. Ed.*, 2021, **60**, 26054–26062.

12 H. Jeong, D. Shin, B. S. Kim, J. Bae, S. Shin, C. Choe, J. W. Han and H. Lee, Controlling the Oxidation State of Pt Single Atoms for Maximizing Catalytic Activity, *Angew. Chem., Int. Ed.*, 2020, **59**, 20691–20696.

13 L. Nie, D. Mei, H. Xiong, B. Peng, Z. Ren, X. I. P. Hernandez, A. DeLaRiva, M. Wang, M. H. Engelhard, L. Kovarik, A. K. Datye and Y. Wang, Activation of surface lattice oxygen in single-atom Pt/CeO2 for low-temperature CO oxidation, *Science*, 2017, **358**, 1419–1423.

14 X. Li, X. I. Pereira-Hernandez, Y. Chen, J. Xu, J. Zhao, C. W. Pao, C. Y. Fang, J. Zeng, Y. Wang, B. C. Gates and J. Liu, Functional CeO_x nanoglues for robust atomically dispersed catalysts, *Nature*, 2022, **611**, 284–288.

15 W. Wan, J. Geiger, N. Berdunov, M. Lopez Luna, S. W. Chee, N. Daelman, N. Lopez, S. Shaikhutdinov and B. Roldan Cuenya, Highly Stable and Reactive Platinum Single Atoms on Oxygen Plasma-Functionalized CeO_2 Surfaces: Nanostructuring and Peroxo Effects, *Angew. Chem., Int. Ed.*, 2022, **61**, e202112640.

16 L. Zhang, Q. Bao, B. Zhang, Y. Zhang, S. Wan, S. Wang, J. Lin, H. Xiong, D. Mei and Y. Wang, Distinct Role of Surface Hydroxyls in Single-Atom Pt_1/CeO_2 Catalyst for Room-Temperature Formaldehyde Oxidation: Acid-Base *Versus* Redox, *JACS Au*, 2022, **2**, 1651–1660.

17 D. Wu, S. Zhou, C. Du, J. Li, J. Huang, H.-X. Shen, A. K. Datye, S. Jiang, J. T. Miller, S. Lin and H. Xiong, The

proximity between hydroxyl and single atom determines the catalytic reactivity of Rh_1/CeO_2 single-atom catalysts, *Nano Res.*, 2024, **17**, 397–406.

18 L. Zhang, B. Zhang, P. Xue, J. Li, Z. Zhang, Y. Yang, S. Wang, J. Lin, H. Liao, Y. Wang, Y. Yao, S. Wan and H. Xiong, The Effect of Pretreatment on the Reactivity of Pd/Al_2O_3 in Room Temperature Formaldehyde Oxidation, *ChemCatChem*, 2021, **13**, 4133–4141.

19 P. Bera, K. R. Priolkar, A. Gayen, P. R. Sarode, M. S. Hegde, S. Emura, R. Kumashiro, V. Jayaram and G. N. Subbanna, Ionic Dispersion of Pt over CeO_2 by the Combustion Method: Structural Investigation by XRD, TEM, XPS, and EXAFS, *Chem. Mater.*, 2003, **15**, 2049–2060.

20 H.-H. Liu, Y. Wang, A.-P. Jia, S.-Y. Wang, M.-F. Luo and J.-Q. Lu, Oxygen vacancy promoted CO oxidation over Pt/CeO_2 catalysts: A reaction at Pt–CeO_2 interface, *Appl. Surf. Sci.*, 2014, **314**, 725–734.

21 H. A. Aleksandrov, K. M. Neyman, K. I. Hadjiivanov and G. N. Vayssilov, Can the state of platinum species be unambiguously determined by the stretching frequency of an adsorbed CO probe molecule?, *Phys. Chem. Chem. Phys.*, 2016, **18**, 22108–22121.

22 X. I. Pereira-Hernandez, A. DeLaRiva, V. Muravev, D. Kunwar, H. Xiong, B. Sudduth, M. Engelhard, L. Kovarik, E. J. M. Hensen, Y. Wang and A. K. Datye, Tuning Pt-CeO_2 interactions by high-temperature vapor-phase synthesis for improved reducibility of lattice oxygen, *Nat. Commun.*, 2019, **10**, 1358.

23 D. Kunwar, S. Zhou, A. DeLaRiva, E. J. Peterson, H. Xiong, X. I. Pereira-Hernández, S. C. Purdy, R. ter Veen, H. H. Brongersma, J. T. Miller, H. Hashiguchi, L. Kovarik, S. Lin, H. Guo, Y. Wang and A. K. Datye, Stabilizing High Metal Loadings of Thermally Stable Platinum Single Atoms on an Industrial Catalyst Support, *ACS Catal.*, 2019, **9**, 3978–3990.

24 P. Xie, T. Pu, A. Nie, S. Hwang, S. C. Purdy, W. Yu, D. Su, J. T. Miller and C. Wang, Nanoceria-supported single-atom platinum catalysts for direct methane conversion, *ACS Catal.*, 2018, **8**, 4044–4048.

25 A. Ankudinov, J. Rehr, J. J. Low and S. R. Bare, Sensitivity of Pt X-ray absorption near edge structure to the morphology of small Pt clusters, *J. Chem. Phys.*, 2002, **116**, 1911–1919.

26 J. Resasco, L. DeRita, S. Dai, J. P. Chada, M. Xu, X. Yan, J. Finzel, S. Hanukovich, A. S. Hoffman and G. W. Graham, Uniformity is key in defining structure–function relationships for atomically dispersed metal catalysts: the case of Pt/CeO_2, *J. Am. Chem. Soc.*, 2019, **142**, 169–184.

27 H. A. Aleksandrov, K. M. Neyman and G. N. Vayssilov, The structure and stability of reduced and oxidized mononuclear platinum species on nanostructured ceria from density functional modeling, *Phys. Chem. Chem. Phys.*, 2015, **17**, 14551–14560.

28 Y. Lu, S. Zhou, C.-T. Kuo, D. Kunwar, C. Thompson, A. S. Hoffman, A. Boubnov, S. Lin, A. K. Datye, H. Guo and A. M. Karim, Unraveling the Intermediate Reaction Complexes and Critical Role of Support-Derived Oxygen Atoms in CO Oxidation on Single-Atom Pt/CeO_2, *ACS Catal.*, 2021, **11**, 8701–8715.

29 H. N. Pham, A. DeLaRiva, E. J. Peterson, R. Alcala, K. Khivantsev, J. Szanyi, X. S. Li, D. Jiang, W. Huang, Y. Sun, P. Tran, Q. Do, C. L. DiMaggio, Y. Wang and A. K. Datye, Designing Ceria/Alumina for Efficient Trapping of Platinum Single Atoms, *ACS Sustainable Chem. Eng.*, 2022, **10**, 7603–7612.

30 D. Donadio, L. M. Ghiringhelli and L. Delle Site, Autocatalytic and cooperatively stabilized dissociation of water on a stepped platinum surface, *J. Am. Chem. Soc.*, 2012, **134**, 19217–19222.

31 Y. Lee, G. He, A. J. Akey, R. Si, M. Flytzani-Stephanopoulos and I. P. Herman, Raman analysis of mode softening in nanoparticle $CeO_{2-\delta}$ and Au-$CeO_{2-\delta}$ during CO oxidation, *J. Am. Chem. Soc.*, 2011, **133**, 12952–12955.

32 D.-Y. Wei, M.-F. Yue, S.-N. Qin, S. Zhang, Y.-F. Wu, G.-Y. Xu, H. Zhang, Z.-Q. Tian and J.-F. Li, *In situ* Raman observation of oxygen activation and reaction at platinum–ceria interfaces during CO oxidation, *J. Am. Chem. Soc.*, 2021, **143**, 15635–15643.

33 X. Sun, J. Lin, H. Guan, L. Li, L. Sun, Y. Wang, S. Miao, Y. Su and X. Wang, Complete oxidation of formaldehyde over TiO_2 supported subnanometer Rh catalyst at ambient temperature, *Appl. Catal., B*, 2018, **226**, 575–584.

34 X. Chen, G. He, Y. Li, M. Chen, X. Qin, C. Zhang and H. He, Identification of a Facile Pathway for Dioxymethylene Conversion to Formate Catalyzed by Surface Hydroxyl on TiO_2-Based Catalyst, *ACS Catal.*, 2020, **10**, 9706–9715.

35 Y. Huo, X. Wang, Z. Rui, X. Yang and H. Ji, Identification of the Nearby Hydroxyls' Role in Promoting HCHO Oxidation over a Pt Catalyst, *Ind. Eng. Chem. Res.*, 2018, **57**, 8183–8189.

